Journal Pre-proofs

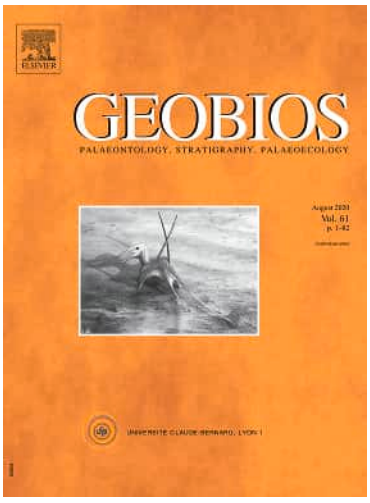

Research Paper

Osteohistology of Enantiornithine Birds from the Lower Cretaceous Xiagou Formation

Jessie Atterholt, Jingmai K. O'Connor, Hailu You

PII: S0016-6995(25)00018-X
DOI: https://doi.org/10.1016/j.geobios.2024.08.020
Reference: GEOBIO 1116

To appear in: *Geobios*

Received Date: 22 November 2023
Revised Date: 13 June 2024
Accepted Date: 5 August 2024

Please cite this article as: J. Atterholt, J.K. O'Connor, H. You, Osteohistology of Enantiornithine Birds from the Lower Cretaceous Xiagou Formation, *Geobios* (2025), doi: https://doi.org/10.1016/j.geobios.2024.08.020

Osteohistology of Enantiornithine Birds from the Lower Cretaceous Xiagou Formation ✡

Jessie Atterholt [a,*], Jingmai K. O'Connor [b,c], Hailu You [c]

[a] College of Osteopathic Medicine of the Pacific, Western University of Health Sciences, Pomona, CA, 91766, U.S.A.

[b] Negaunee Integrative Research Center, Field Museum of Natural History, Chicago, Illinois, 60605, U.S.A.

[c] Key Laboratory of Vertebrate Evolution and Human Origins, Institute of Vertebrate Paleontology and Paleoanthropology, Chinese Academy of Sciences, Beijing, 100044, P. R. China

* Corresponding author. E-mail address: jessie.atterholt@gmail.com (J. Atterholt).

✡ Corresponding editor: Francisco J. Serrano.

Abstract

We describe the osteohistology of five enantiornithine bird specimens from Lower Cretaceous Xiagou Formation deposits of the Changma locality in northwestern Gansu Province, China. Samples were taken from the femora of: three specimens of *Avimaia schweitzerae* (IVPP V25371, IVPP V31956, and GSGM-04-CM-007), *Qiliania graffini* GSGM-04-CM-006, and *Novisavis pubisculata* IVPP V31957. The objective of this study is to describe intrageneric variation (in *Avimaia*), and intertaxonomic variation among enantiornithine birds coexisting in an ecosystem. All five specimens have a femoral cortex composed mainly of parallel fibered bone with relatively low vascularity. All three *Avimaia* specimens have 2-3 vascular canals, and asymmetrical growth marks, indicating cortical drift. In *Qiliania* there are eight longitudinal vascular canals, five of which are concentrated in one region of the cortex. Although the gross anatomy of the skeleton and fusion of compound elements indicates morphological maturity, neither growth marks, an outer circumferential layer (OCL), nor an inner circumferential layer (ICL) are present. The femur of *Novisavis* has some regions of a woven parallel complex and a higher level of vascularity relative to the other specimens (14

longitudinal channels present). Although this specimen is morphologically immature based on gross anatomy, the femur has a well-developed OCL and ICL. These results emphasize the enantiornithine offset between morphological maturity and osteohistological maturity. Development of the OCL appears to be decoupled from morphological maturity, in some cases forming before the skeleton has fully fused, and in others well after. The specimens are similar in size but vary considerably in the number of growth marks present, from none to two. This suggests either developmental plasticity and diverse growth strategies and, complicates attempts to interpret relative age and growth stage in enantiornithines.

Keywords:

Enantiornithes

Mesozoic bird

Osteohistology

Life history traits

1. Introduction

Enantiornithes are the dominant group of terrestrial birds in the Cretaceous with fossils found on every continent except Antarctica (Chiappe and Walker, 2002; O'Connor, 2022). While members of this clade are predominantly arboreal, the fragmentary Late Cretaceous fossil record suggests by this time they had evolved increased ecological diversity (Chiappe and Walker, 2002; O'Connor et al., 2011; O'Connor, 2022). In recent decades with growth in the field of paleo-osteohistology, histological sampling and description of enantiornithine birds has fortunately become increasingly common. From deposits in China in particular, many specimens have been osteohistologically described – e.g., *Zhouornis hani* (CNUVB-0903; Zhang et al., 2013), indeterminate enantiornithine (STM 29-8; O'Connor et al., 2014), *Eopengornis martini* (STM24-1; Wang et al., 2014b), *Parapengornis eurycaudatus* (IVPP V18687; Hu et al., 2015), *Monoenantiornis sihedangia* (IVPP V20289; Hu and O'Connor, 2017), *Pterygornis dapingfangensis* (IVPP V16363; Wang et al., 2017a), *Cruralispennia multidonta* (IVPP V21711; Wang et al., 2017b), indeterminate pengornithid (IVPP V15576A; O'Connor et al., 2018), *Mirusavis parvus* (IVPP V18692; Wang et al., 2020), and *Musiavis amabilis* (MHGU-3000; Wang et al., 2022). These works generally indicate that enantiornithine life history traits were different from those of extant birds, with a prolonged phase of relatively slow growth evidenced by a predominance of poorly-vascularized parallel-fibered bone tissue in many of the long bones of the skeleton (Wang et al., 2014a; Wang et al., 2017a; Wang et al., 2017b), in contrast to the predominance of fibrolamellar bone in crown group birds (Neornithes). Enantiornithines also frequently form growth marks in the cortices of long bones, indicating pauses in growth that are absent in most neornithines (Bourdon et al., 2009; Zhang et al., 2013; O'Connor et al., 2014). However, previous studies also indicate some reproductive similarities with modern birds. Several enantiornithine specimens show evidence that during egg-laying these birds deposited a layer

of medullary bone as a calcium reservoir for eggshell formation (O'Connor et al., 2018; Bailleul et al., 2019; Wang et al., 2020).

Nearly all of the sampled Chinese specimens are from the Lower Cretaceous Jehol deposits in northeastern China, which consist of three successive formations: the Huajiying Fm. in Hebei Province, and the Yixian and Jiufotang formations in Liaoning Province (Pan et al., 2013). Sampling of avian specimens from outcrops in other regions of China is limited to *Avimaia schweitzerae* from the Lower Cretaceous Xiagou Fm. (Bailleul et al., 2019) and *Parvavis chuxiongensis* from the Upper Cretaceous Jiangdihe Fm. (Wang et al., 2014a).

In this study, we present results of an osteohistological analysis of five enantiornithine specimens from the Lower Cretaceous (Aptian) Xiagou Fm. in Gansu Province, northwestern China, from a locality near the town of Changma (Suarez et al., 2013). This site produces fossil bird specimens preserved in slabs, often with three-dimensional skeletal elements. Most of the birds from the site are referable to the ornithuromorph taxon *Gansus yumenensis* (Hou and Liu, 1984; You et al., 2006; Li et al., 2011; Wang et al., 2016), and four additional ornithuromorph taxa have been described (Wang et al., 2013; O'Connor et al., 2022). While less numerous in terms of quantity of specimens, a comparable taxonomic diversity of Enantiornithes has been recovered from the Changma locality. These include *Avimaia schweitzerae* (Lamanna et al., 2006; Bailleul et al., 2019), *Qiliania graffini* (Ji et al., 2011), *Dunhuangia cuii* (Wang et al., 2015), *Feitianius paradisi* (O'Connor et al., 2016), and *Novisavis pubisculata* (O'Connor et al., 2025b).

The specimens that are the subject of this study include the holotype of *Qiliania graffini* (GSGM-04-CM-006), the holotype of *Novisavis pubisculata* (IVPP V31957), the holotype of *A. schweitzerae* (IVPP 25371), a previously referred specimen of *Avimaia* (GSGM-04-CM-007; Lamanna et al., 2006; Bailleul et al., 2019), and a previously undescribed specimen, IVPP V31956, which we refer to *Avimaia* sp. While current research provides a solid foundation for understanding enantiornithine life history characteristics in a general sense, much remains unknown about enantiornithine development at a more granular level, complicating comparisons between individuals of the same taxon or the same ecosystem. For the first time in an enantiornithine, our sampling allows for the study of intrageneric variation (in *Avimaia*), as well as proximodistal serial variation of consecutive thin sections of the diaphysis (in *Avimaia* IVPP 25371). Furthermore, isotope analysis shows that the specimens presented here would have inhabited the same environment, and possibly coexisted in the same ecosystem (Suarez et al., 2017), thus adding important ecological and environmental context to these intertaxonomic comparisons.

2. Material and methods

All five specimens included in this study are reposited at the Institute of Vertebrate Paleontology and Paleoanthropology (IVPP) in Beijing, China. Additionally, all are mostly-articulated skeletal elements preserved in matrix slabs, typical of specimens from the lacustrine deposits of the Changma locality (Harris et al., 2006; Lamanna et al., 2006; You et al., 2006). IVPP V31956 is referrable to *Avimaia* sp. based on the unique delicate and curved morphology of the pubis (an autapomorphy of this taxon) and supported by the morphology and proportions of the foot (see Appendix A for a complete anatomical description and illustration of this specimen). It consists of a partial caudal half of the skeleton, preserving portions of the pelvic girdle, both pubes, the proximal part of the right femur, and the

complete left pelvic limb; this specimen is inferred to be morphologically mature based on the complete fusion of the tarsometatarsus. GSGM-04-CM-007, also referred to *Avimaia*, consists of a fragmentary pelvic girdle and two complete pelvic limbs (Lamanna et al., 2006). It is inferred to be a morphologically mature individual from the complete fusion of the proximal tarsals to the tibia, the distal tarsals to the metatarsals, and the pelvic bones at the level of the acetabulum. IVPP V25371 is the holotype of *Avimaia schweitzeri* (although it was not at the time of sampling for this project). This specimen consists of the caudal half of the axial skeleton, preserving the pelvic girdle, a complete right pelvic limb, and a partial left pelvic limb (Bailleul et al., 2019). On the basis of a fully fused tarsometatarsus, it is inferred to be morphologically mature; furthermore, Bailleul et al. (2019) present evidence that it was also sexually mature (an egg is preserved in the body cavity and medullary bone is present in the femur). However, they also describe the specimen as "skeletally" immature on the basis of osteohistology (Bailleul et al., 2019); it is hereafter described in this paper as "osteohistologically immature" for clarity.

GSGM-04-CM-006 is the holotype specimen of *Qiliania graffini*, consisting of a nearly complete left pelvic girdle and limb, in articulation except for the femur and girdle (Ji et al., 2011). Most of the fossil has been subject to minimal crushing and has remarkable three-dimensional preservation for an avian fossil preserved in a slab such that one limb was able to be prepared free of the sediment; however, the femur from which the histological sample was taken was one of the most damaged elements. Based on the complete fusion of elements of the tibiotarsus and tarsometatarsus, this specimen is inferred to be morphologically mature. IVPP V31957 is the holotype of *Novisavis pubisculata* (O'Connor et al., 2025b). This specimen is also a partial skeleton of the caudal part of the body, including the caudal vertebrae, an incomplete pelvic girdle, and two mostly complete pelvic limbs. Unlike other specimens in this study, the holotype of *Novisavis* is inferred to be at a late stage of morphological immaturity. The skeleton is fully ossified, and while some compound elements have started to fuse, the metatarsals remain separate from one another.

These five specimens were selected for destructive sampling to obtain a maximally diverse taxonomic sample, while restricting damage to specimens that were relatively incomplete compared to other enantiornithine material from Changma. Tissue samples were taken from the mid-shaft of the femur of each specimen at the IVPP, by IVPP technicians. It is common practice in osteohistological studies that aim to explore growth patterns to sample a long bone at the mid-shaft (de Ricqlès et al., 2003; Lamm, 2013; de Buffrénil et al., 2021), an area that typically exhibits symmetrical growth, has been minimally impacted by secondary growth that could obscure evidence of earlier ontogeny, and is a location where the record of growth is likely to be most complete relative to other skeletal elements. Here, we sampled the femur specifically because it was bilaterally preserved in all specimens and because the femur is commonly sampled in other osteohistological studies of enantiornithines (Zhang et al., 2013; O'Connor et al, 2014; Wang et al., 2014b; Hu et al., 2015), thereby allowing for direct comparisons.

These samples were prepared following standard methods for processing osteopaleohistological tissues (Lamm, 2013). They were embedded in epoxy resin, thin-sectioned, and mounted on glass slides at the IVPP. Subsequently, the mounted wafers were ground to approximately 100 μm thickness using a lap grinder (EcoMet 3, Buehler Ltd., Lake Bluff, IL) with descending grits (260-1200) of silica-carbide grit paper using water as a lubricant at the University of California Museum of Paleontology in Berkeley, CA, U.S.A.

Slices were photographed using a Nikon digital sight camera and petrographic microscope (DS-U3 and DS-Fi2), and captured using the computer program NIS-Elements (F4.00.00); and on a Jenoptik camera mounted on an Olympus BX60F. Sections were visualized under regular light and with cross-polarized light (XPL).

All measurements of thin section images were acquired using ImageJ (v.51; National Institute of Health, Bethesda, MD, U.S.A.). We measured cortical width to have a quantifiable variable by which to make comparisons among taxa (Table 1). Cortical width is reported as an average of eight different measurements across the cortex (medially, laterally, cranially, caudally, and four midpoints between these regions). We also include measurements of femoral length for the specimens in this study as a proxy for body size (Table 1), demonstrating the narrow size range occupied by these specimens (ranging from 2.41 to 2.51 cm). Finally, we also include data from a previous study (Atterholt and Woodward, 2021) on two crown group birds: a green-cheeked conure (*Pyrrhura molinae*) and a mourning dove (*Zenaida macroura*). These were chosen because they have a similar femoral length and cortical width to the fossil specimens, with the aim of making comparisons to extant birds with similar biological traits (size and ecology). Both specimens are histologically and morphologically mature.

In this study, we follow the suggestions of Griffin et al. (2021) in using specific nomenclature to describe ontogenetic status as carefully and accurately as possible. Specifically, we use the phrase “morphological maturity” to refer to ontogenetic status based on degree of skeletal fusion and ossification; and “osteohistological maturity” to refer to status as indicated by features of bone tissue and microstructure (see O’Connor et al., 2025a, for a complete discussion of the decoupling of, and definitions for, morphological and osteohistological maturity in enantiornithines).

Abbreviations: **CNUVB**, Capital Normal University, Beijing, China; **GSGM**, Gansu Geological Museum, Lanzhou, China; **IVPP**, Institute of Palaeontology and Palaeoanthropology, Beijing, China; **MHGU**, Museum of Hebei GEO University, Shijiazhuong, China; **MVZ**, Museum of Vertebrae Zoology, Berkeley, CA, United States; **STM**, Shandong Tianyu Museum of Nature, Pingyi, China.

3. Results

3.1. Avimaia schweitzerae *(IVPP V25371, holotype)*

Although the osteohistology of the femur from *Avimaia* IVPP V25371was reported in the original description of the specimen (Bailleul et al., 2019), we include results of a second thin section in the current paper because this provides a rare opportunity to assess serial variation in bone microstructure along the shaft within a single fossil element. The thin section presented here was taken from a position distal to the sample originally described. Although both are from approximately mid-shaft, they are proximal (original sample) and distal (new sample) relative to each other, and these descriptors are used herein to differentiate them.

Unfortunately, and as has been noted in the original description (Bailleul et al., 2019), this element is affected by a microbial invasion that makes it difficult to discern microstructural details. Nonetheless, many features are still clear (Fig. 1(A)). A thin layer of medullary bone lines the endosteal surface and gives off numerous trabecular projections (many of which were broken when this section of the femur was crushed during fossilization). A distinct and well-developed inner circumferential layer (ICL) is present, bounded by a marked resorption line (Fig. 1(B)). A growth line is present, visible in roughly half the cortical circumference but terminating in the ICL at both ends (Fig. 1(C)). The fact that this line is not continuous around the entire cortical circumference is evidence of cortical drift in shaping the growing bone. The few osteocyte lacunae that are discernible throughout the cortex appear very flattened in shape and arranged parallel to the direction of the organized collagen fibers.

There is some notable, if minor, variation between the serial sections. While the proximal section shows at least three longitudinal vascular canals, only one of those appears to have persisted into the region of bone represented by the distal thin section. While the same growth mark reported in the proximal section is still visible, it is in a position even closer to the endosteal margin of the cortex in the distal section. Furthermore, while originally described as a line of arrested growth (LAG), in the distal section the hard line of the "LAG" grades into a more diffuse band, resembling an annulus (Fig. 1(C, D)) This structure is best viewed under polarized light with crossed Nicols, which reveals a band of parallel collagen fibers running in a different direction. Finally, there is a difference in average cortical width (Table 1): the proximal thin section is 179.6 μm thick, while the more distal is 150.5 μm (min: 133.1 μm; max: 176.3 μm).

3.2. Avimaia *sp. (IVPP V31956)*

Fortunately, and unlike many of the other fossils from this site, microstructural preservation of this specimen is excellent. Unfortunately, due to breakage of the very delicate bone during the process of tissue sampling, only two very small portions of the cortex, at nearly opposite poles, remain after sectioning (Fig. 2(A)). Based on these two portions of the cortex, the average cortical width is moderately higher than in the other two *Avimaia* specimens (Table 1), measuring 186.2 μm on average (min: 175.0 μm; max: 197.3 μm).

The preserved cortical bone of this specimen is predominantly composed of parallel-fibered bone that is highly-organized (Fig. 2). An ICL of lamellar bone is present, demarcated by a resorption line (Fig. 2(B, C)), and is especially clear under polarized light with crossed Nicols (Fig. 2(D)). An outer circumferential layer (OCL) also has developed, though less strongly, appearing more similar to the "incipient" OCLs seen in some modern birds (Atterholt and Woodward, 2021; Fig. 2(B, C)). This layer does not contain any growth marks, but instead is characterized by a gradual reduction in number of osteocyte lacunae and extreme flattening of those that are present. It is similar to the thin, weakly-developed OCLs seen in the humerus and femur of undescribed Early Cretaceous enantiornithine specimen STM 29-8 (O'Connor et al., 2014), the humerus of *Cruralispennia multidonta* (IVPP V21711; Wang et al., 2017b), and the humerus, radius, and femur of *Pterygornis dapingfangensis* (IVPP V16363; Wang et al., 2017a).

The preserved portions of this element have very low vascular porosity, with only a single, longitudinal, simple vessel present (Fig. 2(C, D)). Vascularity tends to vary across the

circumference of an enantiornithine bone, and it would thus not be best practice to generally characterize this trait in this specimen based on so little data. However, the preserved portions of the cortex, together with the other *Avimaia* specimens described herein, strongly suggests that vascularity would have been low. Osteocyte lacunae vary in shape throughout the cortex (Fig. 2(B, C)). They are numerous and moderately flattened in the thick middle section, and relatively large and slightly more rounded in the ICL. However, in the OCL they are few in number and extremely compressed in appearance (essentially the only feature distinguishing this outer layer of bone). The quality of preservation is so good that canaliculi are clearly visible around many lacunae, particularly in the endosteal half of the cortex (Fig. 2(C)).

A very clear pair of growth marks is present in the middle layer of one portion of the cortex, but apparently did not continue around the full circumference of the bone, because it is absent in the other preserved fragment (Fig. 2(A-C)), additional evidence of the high variability of some microstructural features in enantiornithines. Although not in a similar position to the growth mark observed in the holotype specimen (which is much closer to the endosteal margin of the cortex), this is also further evidence of the role of cortical drift in shaping the femur in this taxon.

3.3. Avimaia *sp. (GSGM-04-CM-007)*

Extensive crushing and extremely poor preservation (including microbial invasion) make interpretation of this specimen difficult (Fig. 3). Unlike the other two *Avimaia* specimens, cortical width appears much less uniform throughout the circumference of the bone, although this may be an artifact of the low quality of preservation. Nonetheless, it is possible to say that the element was thin-walled with an average cortical width of 120.3 μm (min: 85.2 μm; max: 193.9 μm) and composed completely of parallel-fibered bone (Fig. 3(A)). At this mid-diaphyseal section, the bone is avascular, although small vascular canals could well be obscured by the microbial invasion. An ICL is present, recognizable as a thin layer of highly-organized, nearly acellular bone (Fig. 3(B)). Despite the poor preservation, an endosteal resorption line between the cortical bone and endosteal bone is very clear. Some portions of the cortex seem to have a thin, incipient OCL, appearing as a layer of bone with few osteocyte lacunae (Fig. 3(B)). Osteocyte lacunae all are very flattened in shape as viewed in this transverse plane (Fig. 3(C)). There is at least one irregular growth mark present in one section of the cortex, cutting across obliquely from the periosteal edge to mid-cortex where it terminates in a diffuse way, grading into the parallel-fibered bone of the cortex (Fig. 3(C)). This growth mark asymmetry is similar to that observed in the other two *Avimaia* specimens and other enantiornithines – e.g., pengornithid (IVPP V15576A; O'Connor et al., 2018), indeterminate enantiornithine (STM 29-8; O'Connor et al., 2014), and *Zhouornis hani* (CNUVB-0903; Zhang et al., 2013).

3.4. Qiliania graffini *(GSGM-04-CM-006, holotype)*

Microstructural preservation is poor, showing evidence of a microbial invasion similar to that described in the femur of the holotype of *Avimaia* (Bailleul et al., 2019). Nonetheless, it is clear that the femur of *Qiliania* GSGM-04-CM-006 was very thin-walled and composed of parallel-fibered bone (Fig. 4; Table 1). The average cortical width is 130.8 μm (min: 102.5 μm; max: 191.1 μm). This element has a low level of vascularization. In the whole of the

femoral cortex, eight channels were visible, five of which are concentrated within one region of the cortex, while the others are more dispersed (Fig. 4(A, B)). These vessels are all longitudinally oriented. Osteocyte lacunae are small and generally flattened throughout the cortex (Fig. 4(C)). Both an OCL and ICL are absent, as are any growth marks; however, skeletal ossification and fusion of elements indicate it had completed or was approaching the end of skeletal growth (Ji et al., 2011). The periosteal surface of the thin section is irregular in some areas (Fig. 4(B)), suggesting that the surface of the bone may have weathered away; however, there is a very smooth periosteal margin around one part of the cortex (Fig. 4(C)), indicating that the lack of an OCL may be real and not merely an artifact of poor preservation.

In absence of a growth series, the lack of an OCL in *Qiliania* GSGM-04-CM-006, a morphologically mature individual, leaves interpretation of the bone tissue preserved in this specimen open to question. Namely, is this cortex essentially composed entirely of an OCL, as in osteohistologically mature Anna's hummingbirds (Atterholt and Woodward, 2021)? However, based on evidence from other enantiornithines (both presented here and in other publications), it is most likely that the parallel-fibered bone represents the middle cortical layer, and that an OCL was slow to develop (or perhaps never formed at all in this taxon). Furthermore, although a minute sample size precludes statistical analysis, the length and cortical width of the femur in Anna's hummingbird (0.84 cm and 43.3 μm, respectively; Atterholt and Woodward, 2021) are both substantially lower than the same measurements in *Qiliania* GSGM-04-CM-006 (Table 1); although the latter was a small bird, it does not fall within the extremes represented by the hummingbird. Based on these measurements, *Qiliania* is much more comparable to a green-cheeked conure (Table 1). In this modern taxon the OCL does not entirely dominate the femoral cortex, thus it is not expected that this would occur in *Qiliania* either.

3.5. Novisavis pubisculata *(IVPP V31957, holotype)*

The cortex of the femur of IVPP V31957 is thin-walled (Table 1) with an average cortical width of 134.8 μm (min: 106.2 μm. max: 159.9 μm) and composed of parallel-fibered bone that is avascular in some regions, and parallel-fibered/loosely woven bone with moderate vascularization in others (Fig. 5(A)). There are 14 vascular channels total at the point where the femur was sectioned, giving this element a higher vascularity than the other specimens described in this study. All vascular canals run longitudinally, and many form the central canals of primary osteons (Fig. 5(B, D)). The regions of loosely woven bone with primary osteons form what appear to be areas of a woven parallel complex, sensu Prondvai et al. (2014) (Fig. 5(B, D)). This area closely resembles bone tissue in the femur of a morphologically and osteohistologically mature green-cheeked conure (Fig. 6(A, B)), which also is weakly woven bone with a moderate level of vascularity. Although the avascular, parallel-fibered regions of the cortex of IVPP V31957 are a marked contrast with the conure, it is notable that this specimen shows some regions of tissue indicative of growth rates presumably similar to that of an extant bird of similar body size (based on femoral length).

A thin, yet distinct ICL is present (Fig. 5(C)). An OCL also is present, bounded by a single growth mark near the periosteal margin which likely marks the slowing of appositional growth and transition to development of the OCL (Fig. 5(C)). The ICL, OCL, and growth line are only visible in approximately one half of the cortex, although this discrepancy is probably due to poorer preservation and loss of periosteal bone on the other cortical fragments, which appear less intact along both the endosteal and periosteal margins. The presence of an ICL

and OCL indicates that endosteal resorption and periosteal appositional growth had both ceased, thus the presence of a regional weakly woven bone with primary osteons is noteworthy as it points to the persistence of relatively fast growth in at least some parts of the femur late in ontogeny.

We note that an alternative interpretation of the purported OCL in *Novisavis* is that it may simply represent a relatively short period of growth that resumed after the pause represented by the growth line, and that this layer of bone would have continued to expand as periosteal growth persisted, as is observed in the *Avimaia* specimens described herein, several other enantiornithines – the femur of Early Cretaceous taxon *Zhouornis hani* (CNUVB-0903; Zhang et al., 2013), the femora of two undescribed Argentinian enantiornithines (PVL-4273 and MACN-S-01; Chinsamy et al., 1995), and various skeletal elements of the Late Cretaceous avisaurid taxon, *Mirarce eatoni* (UCMP 139500; Atterholt et al., 2021). In this case, the outer layer of tissue beyond the growth mark in *Novisavis* would not be an OCL. However, two pieces of evidence point to this being a true OCL. Firstly, osteocyte lacunae in this layer are sparser and much more compressed than in the middle cortical layer (and similar to the lacunae in the ICL). Secondly, the average cortical width is already in range of the widths observed in other specimens in this study, and it is therefore very plausible that very little additional appositional growth would have occurred.

4. Discussion

4.1. Serial and intrageneric variation in Avimaia

Relatively little serial variation was observed in the two thin sections from the femur of the *Avimaia* IVPP V25371 presented here. The most notable difference lies in the morphology of the growth mark which presents as a “LAG” in the more proximal section but in the distal section shifts to a much more diffuse appearance, more closely resembling an “annulus”. As noted by others (Cullen et al., 2014; Canoville et al., 2016; Prondvai, 2017; Chapelle et al., 2021; Cullen et al., 2021), this highlights the variability of bone tissue even within the diaphysis of the same element and indicates that interpretations based on single sections should be made cautiously, in light of probable variation both within and between elements. This also emphasizes the difficulty in defining these two terms (“LAG” and “annulus”), and in making inferences regarding the biological significance of the growth mark. The difference in average cortical width between the two thin sections (179.6 μm vs. 150.5 μm) is also notable.

Intrageneric variation in osteohistological characteristics was also minimal, outside of the notable variance in number of preserved growth marks. The three *Avimaia* specimens exhibit a range of cortical widths (Table 1), although the small sample size precludes statistical analysis. However, we note that the inter-element variation in cortical width seen in the *Avimaia* holotype makes this range of variation less remarkable. Taking this into account, the only real stand-out seems to be GSGM-04-CM-007 (average cortical width = 120.3 μm, min = 85.2 μm, max = 193.9 μm), although the thin cortex observed here may be due to poor preservation and furthermore is well within the range of intrageneric variation in cortical width observed in modern birds (Atterholt and Woodward, 2021).

The most notable variation between the three specimens of *Avimaia* lies in the number of growth marks and their location within the cortex. IVPP V31956 has two very distinct

parallel growth marks, resembling LAGs. These have a mid-cortical location, for the portions of the section in which they are visible. In contrast, IVPP V25371 and GSGM-04-CM-007 only preserve one mark each; in both, this mark appears to transition from a hard, clear line (similar to a "LAG") to a wider, more diffuse band (similar to an "annulus"). In IVPP V25371, the growth mark is located near the endosteal margin of the cortex. In GSGM-04-CM-007, the growth mark is located near the periosteal margin. The analysis of serial variation in IVPP V25371 serves as a reminder that position of a growth mark can shift within the cortex, and this would be particularly expected in the case of the asymmetrical marks observed in all three specimens of *Avimaia*. However, the shifting of position of the marks and their lack of circumferential continuity is suggestive of the importance of cortical drift in shaping the gross morphology of the femur in this taxon. Furthermore, the observed range of number of growth marks is unusual considering the similar body size of the three *Avimaia* specimens; the individual with two growth marks has a femoral length only fractionally larger than the other two (Table 1). This variation in number and position of growth marks suggests growth plasticity as observed in other non-ornithuromorph avians (Chinsamy et al., 2020; O'Connor et al., 2025a), but also may be indicative of seasonal environment fluctuations (although the lack of growth marks in other specimens suggests another cause, see below for further discussion) or sex specific differences in life history such as the energetic imposition of reproduction on female specimens (IVPP V25371). Additionally, the presence of two closely spaced growth marks in IVPP V31956 may be indicative of a major life event such as the onset of reproduction; this may permit hypotheses regarding sex based on osteohistology in the future.

4.2. General remarks on Enantiornithine life history

Osteohistological study of these five specimens overall shows a marked lack of variation in terms of very general microstructural features, considering the representation of three separate taxa, as well as a (modest) range of growth stages as inferred from skeletal fusion and from the histological data (including one late-stage osteohistologically immature specimen and one late-stage morphologically immature specimen). Like the bone described in many other enantiornithines (Chinsamy et al., 1995; Zhang et al., 2013; O'Connor et al., 2014; Wang et al., 2014a; Wang et al., 2017a, 2017b; Wang et al., 2020), all but one can be broadly characterized as composed of parallel-fibered bone, and all have low-to-moderate levels of vascularity. It is important to note that some structures are highly variable around the circumference of a single cortical cross-section. Specifically, vascular canals, growth marks, and the OCL were found to be variably present in most of the thin sections presented here. This underscores the importance of using caution when drawing conclusions based on a fragmentary sample. Furthermore, variation in the number of growth marks is particularly notable, given that all specimens are of a very similar body size. This, in turn, emphasizes the importance of using caution when attempting to interpret growth trajectories based on individual specimens (Cullen et al., 2014; Canoville et al., 2016; Prondvai, 2017; Chapelle et al., 2021; Cullen et al., 2021). Observed differences in growth mark number and development of the OCL and ICL indicate substantive divergence in developmental trajectories prior to the ontogenetic stages represented by these specimens, despite general similarities in bone tissue type and vascularity.

These results also serve to highlight differences between enantiornithine and crown bird life history traits. All individuals represented in this study show evidence that these enantiornithine taxa had an extended period of relatively slow growth (as compared to

modern birds) in the latter part of their developmental trajectories, as indicated by the parallel-fibered tissue of their femora. In *Avimaia* this protracted slow growth may have extended over two or more years, as suggested by the presence of growth marks. However, the absence of growth marks in the morphologically mature *Qiliania* suggests that adult size in this taxon may have been reached in less than a year or that the slow growth phase during later ontogeny was more steady without any pauses, relative to *Avimaia*. This indicates that a diversity of growth trajectories was utilized by sympatric small bodied Early Cretaceous enantiornithines.

It is also worth noting that the specimens in this study preserve bone tissue that is not entirely distinct from neornithines in certain aspects. In crown group birds, Atterholt and Woodward (2021) described an osteohistological trend toward decreasing levels of vascularity and increased levels of bone matrix organization in correlation with decreasing body size; smaller-bodied birds did not have the well-developed fibrolamellar complexes that so often are generally described as characteristic of crown-group bird bone(Chinsamy and Elzanowski, 2001). Instead, these smaller taxa often had cortices with only weakly woven matrices and few simple vascular canals or incipient primary osteons. Furthermore, these patterns which correlated so clearly with body size were independent of developmental mode and dominant locomotor module. This is consistent with the previous observation that differences in bone tissue in early birds compared to large bodied non-avian dinosaurs reflects the relatively smaller body size of stem birds (Erickson et al., 2009). Because of this clear trend in modern birds, and because the birds included in this study are all of small body size, the latter is an important factor to take into consideration when interpreting osteohistological observations. For this reason, we make comparisons with two extant taxa (the green-cheeked conure and mourning dove) with similar femoral length to the Changma enantiornithines (Table 1).

In terms of cortical width, two of the *Avimaia* specimens (IVPP V25371 and IVPP V31956) are very similar to the green-cheeked conure femur. The third *Avimaia* specimen (GSGM-04-CM-007), as well as *Qiliania* and *Novisavis* have thinner femoral cortices than either the green-cheeked conure or the mourning dove. *Qiliania* is broadly comparable to histological attributes seen in the femur of mourning dove (Fig. 6(C, D); Table 1). Like *Qiliania*, the dove is characterized by very low levels of vascularity in the femur (although there are no avascular portions of the cortex). Additionally, it has a middle layer of bone that is weakly woven bordering on parallel-fibered, similar to the parallel-fibered cortex of *Qiliania*. Of course, the bone tissue of *Qiliania* is not identical to the mourning dove bone tissue; *Qiliania* has some regions of the cortex that are more distinctively parallel-fibered, and vascular canals are more regionally concentrated. Nonetheless, it bears discussing how similar the tissue of these stem birds is to that of a small-bodied crown bird, which suggest that the bone histology of such small enantiornithines is at least partially due to their small body size.

The region of a weakly woven bone with primary osteons in *Novisavis* IVPP V31957 is also similar to osteohistological characteristics seen in small-bodied modern birds of an approximately similar size, such as the green-cheeked conure (Fig. 6(A, B)). This indicates that although many enantiornithine birds had life history regimes clearly divergent from crown group birds, they differences are not dichotomous. Here, we see an enantiornithine specimen in a relatively late stage of morphological immaturity and with evidence of osteohistological maturity, presenting tissue in some areas of the cortex very similar to a modern bird. The presence of this weakly woven bone with primary osteons, at least regionally, indicates this taxon seems to have had relatively high rates of growth persisting later in ontogeny or an abbreviated period of slow growth, compared to *Avimaia* and *Qiliania.*

Data presented here also emphasize the enantiornithine offset between morphological maturity (as indicated by the degree of ossification and fusion of the skeleton) and bone tissue maturity (as indicated by osteohistological features). In particular, development of the OCL appears to be decoupled from maturity as indicated by gross morphology, in some cases beginning to form before the skeleton has fully fused (as in IVPP V31957), and in others developing well after, or perhaps never forming at all (as in *Qiliania* GSGM-04-CM-006). This is not surprising, as recent evidence shows the OCL may be present (incipient or fully-formed) in immature growth stages of some crown group birds (Atterholt and Woodward, 2021). In some small-bodied taxa (Anna's hummingbird and house finch), a well-developed OCL has been observed as early as the "fledgling" stage (classified as such on the basis of plumage).

With the extended period of relatively slow growth documented in the ontogeny of so many enantiornithines (Chinsamy et al., 1995; Zhang et al., 2013; O'Connor et al., 2014; Wang et al., 2014a; Wang et al., 2017a, 2017b; Wang et al., 2020), it is also a possibility that a distinct OCL never truly forms in some taxa (although an OCL is present in others, such as *Novisavis* described here and the large bodied Late Cretaceous enantiornithine *Mirarce eatoni*; Atterholt et al., 2021). If slow growth, depositing parallel-fibered bone, comes to a gradual halt an OCL would not necessarily be evident as an obvious and distinct microstructural feature. This is arguably supported by enantiornithine specimens that are morphologically mature, yet show no OCL (*Qiliania* GSGM-04-CM-006) or merely a thin, "incipient" OCL (such as the *Avimaia* specimens described here).

This complicates attempts to interpret relative age and growth stage in enantiornithines, as the OCL cannot necessarily be interpreted as an indicator of "maturity". The importance of distinguishing between "sexual" and "somatic" maturity is becoming increasingly well established (e.g., Chinsamy et al., 2020), as an organism may attain reproductive capacity prior to the cessation of somatic growth, as is demonstrated in dinosaurs including enantiornithines (O'Connor et al., 2018; Bailleul et al., 2019). This subject, together with a parsing of the nomenclature used to describe ontogenetic stage and level of maturity, has recently been discussed at length by Griffin et al. (2021) with respect to saurian reptiles. The results presented here emphasize the importance of their suggestion to eschew traditional terms such as "adult" and "juvenile" in favor of more intentional and specific descriptors (such as "morphologically mature" or "histologically mature"). For example, in the current study *Qiliania* GSGM-04-CM-006 exhibits a greater degree of morphological maturity than *Novisavis* IVPP V31957 as evidenced by the complete fusion of the tarsals to the tibia and metatarsals and fusion of the pelvis at the level of the acetabulum. However, IVPP V31957 is more mature in terms of bone tissue, with a fully-developed OCL. Similarly, all three specimens of *Avimaia* are morphologically mature (with complete fusion of the compound bones including the tibiotarsus and tarsometatarsus). However, only two specimens have an incipient OCL (GSGM-04-CM-007 and IVPP V31956), suggesting they are relatively more osteohistologically mature than IVPP V25371, in which an OCL is absent. IVPP V25371 is intermediate in size between these two specimens indicating developmental plasticity may be responsible for size differences that do not reflect maturity as well as the discord between anatomical and osteohistological maturity. It is also notable that, despite the clear morphological maturity of all three *Avimaia* specimens, the OCL is absent or only weakly developed – a clear unambiguous OCL is not present in any of the individuals studied here.

This study also allows for comparisons among three different taxa of similar body size living in the same environment, and likely even co-existing in the same ecosystem, in or near a closed lake basin with an average mean annual air temperatures of 20.2°C that experienced

seasonally warm and arid conditions but precipitation levels high enough to support abundant plant life in the lake (Suarez et al., 2017). Furthermore, while a detailed study aimed at understanding the ecological adaptations of these taxa has not been undertaken, their small body size, pedal proportions (lengthening distally), and curved pedal ungual morphology strongly suggest that they were all arboreal birds (Hopson, 2001). It is thus notable that, despite evidence of environmental dry-wet seasonality, mid-cortical growth marks (indicative of a slowing or cessation of growth) are present consistently in all three sampled specimens of *Avimaia*, but absent in *Qiliania* GSGM-04-CM-006, in which there are no growth marks at all. In *Novisavis* IVPP V31957, the single growth mark present is associated with the slowing of appositional growth that comes with development of the OCL. This, together with the similar body size of these taxa, suggests each was characterized by unique developmental trajectories. If periosteal deposition and endosteal resorption were still active in *Qiliania* GSGM-04-CM-006 (as suggested by the seeming lack of an OCL and ICL), it is possible that growth marks would have developed later in ontogeny and may have been close to the periosteal margin as in *Novisavis* IVPP V31957. This would also mean that the fusion of the tarsometatarsus does not indicate a cessation of growth in enantiornithines as it does in neornithines. However, the femoral bone of *Qiliania* GSGM-04-CM-006 does shows a record of persistent slow growth, which presumably would have allowed ample time for the formation of seasonal or environmentally-related growth lines. Another possible interpretation of the lack of mid-cortical growth marks in *Qiliaina* and *Novisavis* is that these taxa engaged in migratory behaviors and did not spend the entire year in an environment with seasonal variability that causes pauses in growth (while *Avimaia* did), although such a hypothesis would need to be tested with future isotopic studies. Ultimately, characteristics such as growth marks can be highly variable (Heck and Woodward, 2021) and these conclusions are tentative until a time when sampling of additional specimens of *Qiliania* (and *Novisavis*) might be possible.

5. Conclusions

Collectively, the five specimens and three taxa in this study show a notable variation in femoral osteohistology, considering their similar body size and common environment (and likely also ecosystem). While all have parallel-fibered bone to a greater or lesser degree and generally low vascularity, there are notable differences in the presence and number of growth marks, the formation of an OCL or ICL, and even in bone texture with some having regional weakly woven matrices with a moderate level of vascularity. Furthermore, going beyond these intertaxonomic differences, there is a predominant pattern of osteohistovariability observed in individual thin-sections. We document a “LAG” changing to an “annulus”, growth lines present in part of the cortex and absent in the rest, and regions of vascularity and avascularity, each within a single cross-section of a single element. Although limitations due to poor preservation and the general reluctance to destructively sample fossil specimens means that fragmentary samples may be unavoidable, we urge caution when drawing broad conclusions from an incomplete cortical cross-section. Finally, when complete cross-sections are available, we urge authors to describe and publish photos of entire cross-sections.

CRediT Author Statement

Jessie Atterholt: Conceptualization, Methodology, Validation, Investigation, Resources, Writing (original draft, review & editing), Visualization, Funding Acquisition. Jingmai K. O'Connor: Validation, Investigation, Writing (review & editing). Hailu You: Resources.

Acknowledgements

We express our gratitude to the IVPP for allowing access to the specimens and for permitting destructive sampling. We are grateful to the technicians at the IVPP who collected the tissue samples, and Dr. Shukang Zhang, who embedded and sectioned them, and mounted the wafers on slides. Dr. Lucas Legendre and an anonymous reviewer provided very helpful constructive criticism; this paper is greatly improved thanks to their comments. Thanks to the Jurassic Foundation for funding this research. HLY was supported by the National Natural Science Foundation of China (Grant No. 42288201, 42372030). Finally, a special thank-you to Dr. Jack Horner for allowing use of his microscope for the viewing and describing the thin sections.

Appendix A. Supplementary information

Supplementary information (including the morphological description and illustration of *Avimaia* sp. – IVPP V31956) associated with this article can be found, in the online version, at:

References

Atterholt, J., Poust, A.W., Erickson, G.M., O'Connor, J.K., 2021. Intraskeletal osteohistovariability reveals complex growth strategies in a Late Cretaceous enantiornithine. Frontiers in Earth Science 9, 118.

Atterholt, J., Woodward, H.N., 2021. A histological survey of avian post-natal skeletal ontogeny. PeerJ 9, e12160.

Bailleul, A.M., O'Connor, J., Zhang, S., Li, Z., Wang, Q., Lamanna, M.C., Zhu, X., Zhou, Z., 2019. An Early Cretaceous enantiornithine (Aves) preserving an unlaid egg and probable medullary bone. Nature Communications 10, 1275.

Bourdon, E., Castanet, J., De Ricqlès, A., Scofield, P., Tennyson, A., Lamrous, H., Cubo, J., 2009. Bone growth marks reveal protracted growth in New Zealand kiwi (Aves, Apterygidae). Biology Letters 5, 639–642.

Canoville, A., de Buffrénil, V., Laurin, M., 2016. Microanatomical diversity of amniote ribs: an exploratory quantitative study. Biological Journal of the Linnean Society 118, 706–733.

Chapelle, K.E., Botha, J., Choiniere, J.N., 2021. Extreme growth plasticity in the early branching sauropodomorph Massospondylus carinatus. Biology Letters 17, 20200843.

Chiappe, L.M., Walker, C.A., 2002. Skeletal morphology and systematics of the Cretaceous Euenantiornithes (Ornithothoraces: Enantiornithes). In: Chiappe, L.M., Witmer, L.M. (Eds.), Mesozoic Birds: Above the Heads of Dinosaurs. University of California Press, Berkeley, pp. 240–267.

Chinsamy, A., Chiappe, L.M., Dodson, P., 1995. Mesozoic avian bone microstructure: Physiological implications. Paleobiology 21, 561–574.

Chinsamy, A., Elzanowski, A., 2001. Evolution of growth pattern in birds. Nature 412, 402–403.

Chinsamy, A., Marugán-Lobón, J., Serrano, F.J., Chiappe, L., 2020. Osteohistology and life history of the basal pygostylian, *Confuciusornis sanctus*. The Anatomical Record 303, 949–962.

Cullen, T.M., Brown, C.M., Chiba, K., Brink, K.S., Makovicky, P.J., Evans, D.C., 2021. Growth variability, dimensional scaling, and the interpretation of osteohistological growth data. Biology Letters 17, 20210383.

Cullen, T.M., Evans, D.C., Ryan, M.J., Currie, P.J., Kobayashi, Y., 2014. Osteohistological variation in growth marks and osteocyte lacunar density in a theropod dinosaur (Coelurosauria: Ornithomimidae). BMC Evolutionary Biology 14, 231.

de Buffrénil, V., Quilhac, A., Castanet, J., 2021. Cyclical Growth and Skeletochronology. In: de Buffrénil, V., Zylberberg, L., de Ricqlès, A., Padian, K. (Eds.), Vertebrate Skeletal Histology and Paleohistology. CRC Press, Boca Raton, pp. 626–644.

de Ricqlès, A., Padian, K., Horner, J., Lamm, E., Myhrvold, N., 2003. Osteohistology of *Confuciusornis sanctus* (Theropoda : Aves). Journal of Vertebrate Paleontology 23, 373–386.

Erickson, G.M., Rauhut, O.W.M., Zhou, Z.-H., Turner, A.H., Inouye, B.D., Hu, D.-Y., Norell, M.A., 2009. Was dinosaurian physiology inherited by birds? Reconciling slow growth in Archaeopteryx. PLoS ONE 4, e7390.

Griffin, C.T., Stocker, M.R., Colleary, C., Stefanic, C.M., Lessner, E.J., Riegler, M., Formoso, K., Koeller, K., Nesbitt, S.J., 2021. Assessing ontogenetic maturity in extinct saurian reptiles. Biological Reviews 96, 470–525.

Harris, J.D., Lamanna, M.C., You, H.-l., Ji, S.-a., Ji, Q., 2006. A second enantiornithean (Aves: Ornithothoraces) wing from the Early Cretaceous Xiagou Formation near Changma, Gansu Province, People's Republic of China. Canadian Journal of Earth Sciences 43, 547–554.

Heck, C.T., Woodward, H.N., 2021. Intraskeletal bone growth patterns in the North Island Brown Kiwi (Apteryx mantelli): Growth mark discrepancy and implications for extinct taxa. Journal of Anatomy 239, 1075–1095.

Hopson, J.A., 2001. Ecomorphology of avian and nonavian theropod phalangeal proportions: Implications for the arboreal versus terrestrail origin of bird flight. New Perspectives on the Origin and Early Evolution of Birds, pp. 211–235.

Hou, L., Liu, Z., 1984. A new fossil bird from the Lower Cretaceous of Gansu and early evolution of birds. Scientia Sinica, B 27, 1296–1302.

Hu, H., O'Connor, J.K., 2017. First species of Enantiornithes from Sihedang elucidates skeletal development in Early Cretaceous enantiornithines. Journal of Systematic Palaeontology 15, 909–926.

Hu, H., O'Connor, J.K., Zhou, Z., 2015. A new species of Pengornithidae (Aves: Enantiornithes) from the Lower Cretaceous of China suggests a specialized scansorial habitat previously unknown in early birds. PLoS One 10, e0126791.

Ji, S., Atterholt, J., O'Connor, J.K., Lamanna, M.C., Harris, J.D., Li, D., You, H., Dodson, P., 2011. A new, three-dimensionally preserved enantiornithine bird (Aves: Ornithothoraces) from Gansu Province, north-western China. Zoological Journal of the Linnean Society 162, 201–219.

Lamanna, M.C., You, H.-l., Harris, J.D., Chiappe, L.M., Shu-An, J., Lu, J.-c., Qiang, J., 2006. A partial skeleton of an enantiornithine bird from the Early Cretaceous of northwestern China. Acta Palaeontologica Polonica 51, 423–434.

Lamm, E.-T., 2013. Preparation and Sectioning of Specimens. In: Padian, K., Lamm, E.-T. (Eds.), Bone Histology of Fossil Tetrapods: Advancing Methods Analysis, and Interpretation. University of California Press, pp. 55–160.

Li, Y., Zhang, Y., Zhou, Z., Li, Z., Liu, D., Wang, X., 2011. New material of Gansus and a discussion of its habit. Vertebrata PalAsiatica 49, 435–445.

O'Connor, J., Erickson, G.M., Norell, M., Bailleul, A.M., Hu, H., Zhou, Z., 2018. Medullary bone in an Early Cretaceous enantiornithine bird and discussion regarding its identification in fossils. Nature Communications 9, 5169.

O'Connor, J.K., 2022. Primer: Enantiornithes. Current Biology 32, R1042-R1072.

O'Connor, J.K., Atterholt, J., Bailleul, A.M., Wang, M., Kuo, P.-C., Zhonghe, Z., 2025a. Description and osteohistology of two early immature enantiornithines (Aves: Ornithothoraces) from the Early Cretaceous Jehol Biota. Geobios 90 (in press).

O'Connor, J.K., Atterholt, J., Clark, A.D., Zhou, L., Peng, C., Zhang, X., You, H., 2025b. Enantiornithine (Aves: Ornithothoraces) from the Lower Cretaceous Xiagou Formation with an unusually short pubis. Geobios 90 (in press).

O'Connor, J.K., Chiappe, L.M., Bell, A., 2011. Pre-modern birds: avian divergences in the Mesozoic. In: Dyke, G.D., Kaiser, G. (Eds.), Living Dinosaurs: the Evolutionary History of Birds. J. Wiley & Sons, Hoboken, NJ, pp. 39–114.

O'Connor, J.K., Li, D.-Q., Lamanna, M.C., Wang, M., Harris, J.D., Atterholt, J., You, H.-L., 2016. A new Early Cretaceous enantiornithine (Aves, Ornithothoraces) from northwestern China with elaborate tail ornamentation. Journal of Vertebrate Paleontology 36, e1054035.

O'Connor, J.K., Stidham, T.A., Harris, J.D., Lamanna, M.C., Bailleul, A.M., Hu, H., Wang, M., You, H.L., 2022. Avian skulls represent a diverse ornithuromorph fauna from the

Lower Cretaceous Xiagou Formation, Gansu Province, China. Journal of Systematics and Evolution 60, 1172–1198.

O'Connor, J.K., Wang, M., Zheng, X.-T., Wang, X.-L., Zhou, Z.-H., 2014. The histology of two female Early Cretaceous birds. Vertebrata PalAsiatica 52, 112–128.

Pan, Y.-H., Sha, J.-G., Zhou, Z.-H., Fürsich, F.T., 2013. The Jehol Biota: Definition and distribution of exceptionally preserved relicts of a continental Early Cretaceous ecosystem. Cretaceous Research 44, 30–38.

Prondvai, E., 2017. Medullary bone in fossils: function, evolution and significance in growth curve reconstructions of extinct vertebrates. Journal of evolutionary biology 30, 440–460.

Prondvai, E., Stein, K.H., De Ricqlès, A., Cubo, J., 2014. Development-based revision of bone tissue classification: the importance of semantics for science. Biological Journal of the Linnean Society 112, 799–816.

Suarez, M.B., Ludvigson, G.A., Gonzalez, L.A., Al-Suwaidi, A.H., You, H.-L., 2013. Stable isotope chemostratigraphy in lacustrine strata of the Xiagou Formation, Gansu Province, NW China. In: Bojar, A.-V., Melinte-Dobrinescu, M.C., Smit, J. (Eds.), Isotopic Studies in Cretaceous Research. Geological Society, London.

Suarez, M.B., Ludvigson, G.A., González, L.A., You, H.-L., 2017. Continental paleotemperatures from an early cretaceous dolomitic lake, Gansu Province, China. Journal of Sedimentary Research 87, 486–499.

Wang, M., Li, D., O'Connor, J.K., Zhou, Z., You, H., 2015. Second species of enantiornithine bird from the Lower Cretaceous Changma Basin, northwestern China with implications for the taxonomic diversity of the Changma avifauna. Cretaceous Research 55, 56–65.

Wang, M., Li, Z., Zhou, Z., 2017a. Insight into the growth pattern and bone fusion of basal birds from an Early Cretaceous enantiornithine bird. Proceedings of the National Academy of Sciences of the U.S.A. 114, 11470–11475.

Wang, M., O'Connor, J.K., Bailleul, A.M., Li, Z., 2020. Evolution and distribution of medullary bone: evidence from a new Early Cretaceous enantiornithine bird. National Science Review 7, 1068–1078.

Wang, M., O'Connor, J.K., Pan, Y., Zhou, Z., 2017b. A bizarre Early Cretaceous enantiornithine bird with unique crural feathers and an ornithuromorph plough-shaped pygostyle. Nature Communications 8, 14141.

Wang, M., Zhou, Z., Xu, G., 2014a. The first enantiornithine bird from the Upper Cretaceous of China. Journal of Vertebrate Paleontology 34, 135–145.

Wang, X., Cau, A., Luo, X., Kundrát, M., Wu, W., Ju, S., Guo, Z., Liu, Y., Ji, Q., 2022. A new bohaiornithid-like bird from the Lower Cretaceous of China fills a gap in enantiornithine disparity. Journal of Paleontology 96, 961–976.

Wang, X., O'Connor, J., Zheng, X., 2014b. New information on the evolution of rachis dominated tail feathers from a new basal enantiornithine. Biological Journal of the Linnean Society 113, 805–819.

Wang, Y.-M., O'Connor, J.K., Li, D.-Q., You, H.-L., 2013. Previously unrecognized ornithuromorph bird diversity in the Early Cretaceous Changma Basin, Gansu Province, northwestern China. PLoS One 8, e77693.

Wang, Y.-M., O'Connor, J.K., Li, D.-Q., You, H.-L., 2016. New information on postcranial skeleton of the Early Cretaceous *Gansus yumenensis* (Aves: Ornithuromorpha). Historical Biology 28, 666–679.

You, H.-l., Lamanna, M.C., Harris, J.D., Chiappe, L.M., O'Connor, J., Ji, S.-a., Lu, J.-c., Yuan, C.-x., Li, D.-q., Zhang, X., Lacovara, K.J., Dodson, P., Ji, Q., 2006. A nearly modern amphibious bird from the early Cretaceous of Northwestern China. Science 312, 1640–1643.

Zhang, Z., Chiappe, L.M., Han, G., Chinsamy, A., 2013. A large bird from the Early Cretaceous of China: new information on the skull of enantiornithes. Journal of Vertebrate Paleontology 33, 1176–1189.

Table and Figure captions

Table 1. Measurements from specimens of fossil (identified by a "†" symbol) and extant taxa described and referenced in this study, including femoral length (in specimens with at least one complete femur). Also shown are average cortical width, and minimum and maximum cortical width (in parentheses). For the *Avimaia* holotype specimen (IVPP V25371) average cortical width is given both for the original section described by Bailleul et al. (2019) and for the new section described herein, respectively; minimum and maximum cortical width measurements are reported for the latter.

Taxon	Femoral Length (cm)	Average Cortical Width (µm) (min; max)
Avimaia schweitzerae† (IVPP V25371)	2.52	179.6; 150.5 (133.1; 176.3)

Avimaia sp.† (IVPP V31956)	2.58	186.2 (175.0; 197.3)
Avimaia sp.† (GSGM-04-CM-007)	2.42	120.3 (85.2; 193.9)
Qiliania graffini† (GSGM-04-CM-006)	2.41	130.8 (102.5; 191.1)
Novisavis pubisculata† (IVPP V31957)	—	134.8 (106.2; 159.9)
Green-cheeked conure, *Pyrrhura molinae* (MVZ 190917)	2.61	184.8 (130.1; 247.6)
Mourning dove, *Zenaida macroura* (MVZ 190775)	2.87	229.6 (208.4; 246.8)

Figure 1. Osteohistology of a new thin section sampled from the holotype specimen of *Avimaia schweitzeri* (IVPP V25371). **A.** Entire thin-section showing crushing of the cortex. White box: close-up in Panel B; black box: close-up in Panel C; polarized light. **B.** Portion of the cortex showing a region of avascular, parallel-fibered bone and degree of microbial invasion that obscures details; the ICL is also visible (white arrows); plane light. **C.** Region of the cortex showing the single growth mark, appearing diffuse and similar to an "annulus" (black arrows); polarized light. **D.** Region of the cortex from the originally-published thin section (Bailleul et al., 2019) showing the more LAG-like appearance of the growth mark (black arrows) and the ICL (white arrows); plane light. Scale bars: 100 µm (A, C, D), 50 µm (B).

Figure 2. Osteohistology of referred *Avimaia* specimen IVPP V31956. **A.** Entire cortical cross-section, showing three-dimensional preservation of the femur and the two remaining fragments of cortex; polarized light. **B.** Close-up of region without growth marks, showing a weakly formed or incipient OCL (gray arrows) and an ICL (white arrows); plane light. **C.** Close-up of region with double growth marks (black arrows), also showing the single preserved vascular canal, ICL (white arrows) and OCL (gray arrows); plane light. **D.** Region in panel C shown under polarized light. Scale bars: 250 µm (A), 50 µm (B-D).

Figure 3. Femoral thin section of referred *Avimaia* specimen FRDC-04-CM-007. **A.** Entire thin-section, showing crushing of the cortex and variable cortical width. White box: close-up in panel B; black box: close-up in panel C; plane light. **B.** Portion of the cortex showing poor

microanatomical preservation due to microbial invasion, but with a clear ICL (white arrows) and incipient OCL still visible (gray arrows); plane light. **C.** Portion of the cortex showing the single, asymmetrical growth mark in this element (black arrows), with parallel-fibered bone and osteocyte lacunae visible. White arrows: ICL; plane light. Scale bars: 100 µm (A), 50 µm (B, C).

Figure 4. Femoral thin section of the holotype specimen of *Qiliania graffini* (FRDC-04-CM-007). **A.** Entire cross-section showing a crushed cortex composed of parallel-fibered bone with low vascularity and with canals concentrated only in some regions rather than dispersed evenly throughout. White box: close-up in panel B; black box: close-up in Panel C; polarized light. **B.** Region with a relatively high concentration of vascular canals and scalloped periosteal margin (top left border); plane light. **C.** Region of avascular, parallel-fibered bone with a smooth periosteal margin (bottom right border); the lack of and OCL, ICL, and growth marks is notable relative to the other specimens in this study; plane light. Scale bars: 250 µm (A), 50 µm (B, C).

Figure 5. Osteohistolgy of the femur of *Novisavis pubisculata*. **A.** Complete thin section, showing crushing of the cortex and displacement into two halves. White box: close-up in Panel B; black box: close-up in Panel C; gray box: close-up in Panel D; plane light. **B.** Region of weakly woven bone with primary osteons; plane light. **C.** Region of parallel-fibered bone, in which the OCL (gray arrows) and ICL (white arrows) are very clearly visible; plane light. **D.** Region of the cortex with moderate vascularity, including some weakly-formed primary osteons; plane light. Scale bars: 250 µm (A), 50 µm (B-D).

Figure 6. Osteohistology of the femur from osteohistologically- and morphologically-mature individuals of two neornithine taxa, showing aspects of bone microstructure similar to that of the enantiornithines presented here. **A, B.** Green-cheeked conure (MVZ 190917) with weakly-formed fibrolamellar bone. **C, D.** Mourning dove (MVZ 190775) showing low levels of vascularity and a middle cortical layer formed of bone that is weakly woven, bordering on parallel-fibered. Gray arrows indicate an OCL, and white arrows indicate an ICL. Images in panels A, C, and D shown under plane light, and that in B under polarized light. All sections stained with toluidine blue. Scale bars: 50 µm.

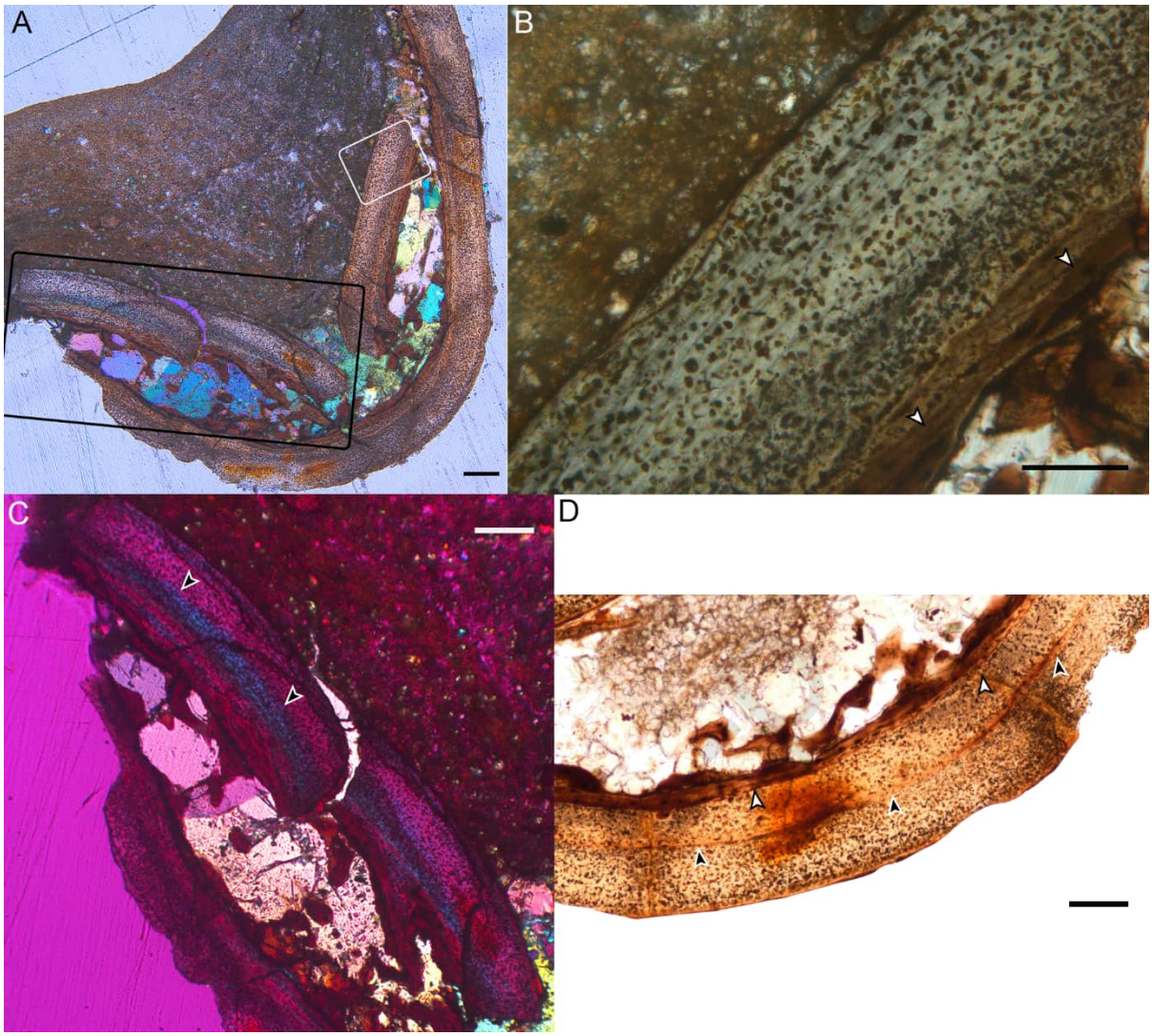
A
B
C
D

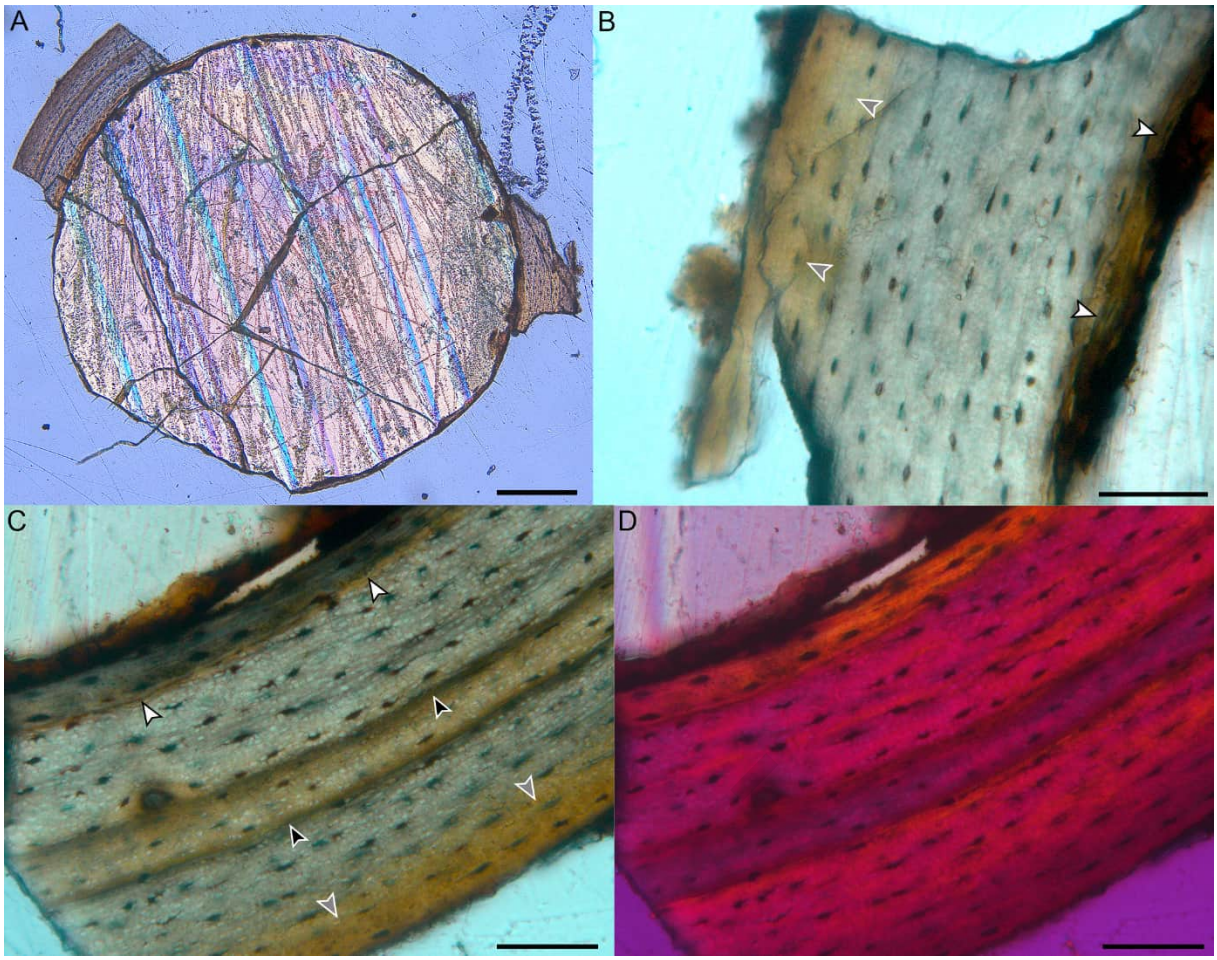
A
B
C
D

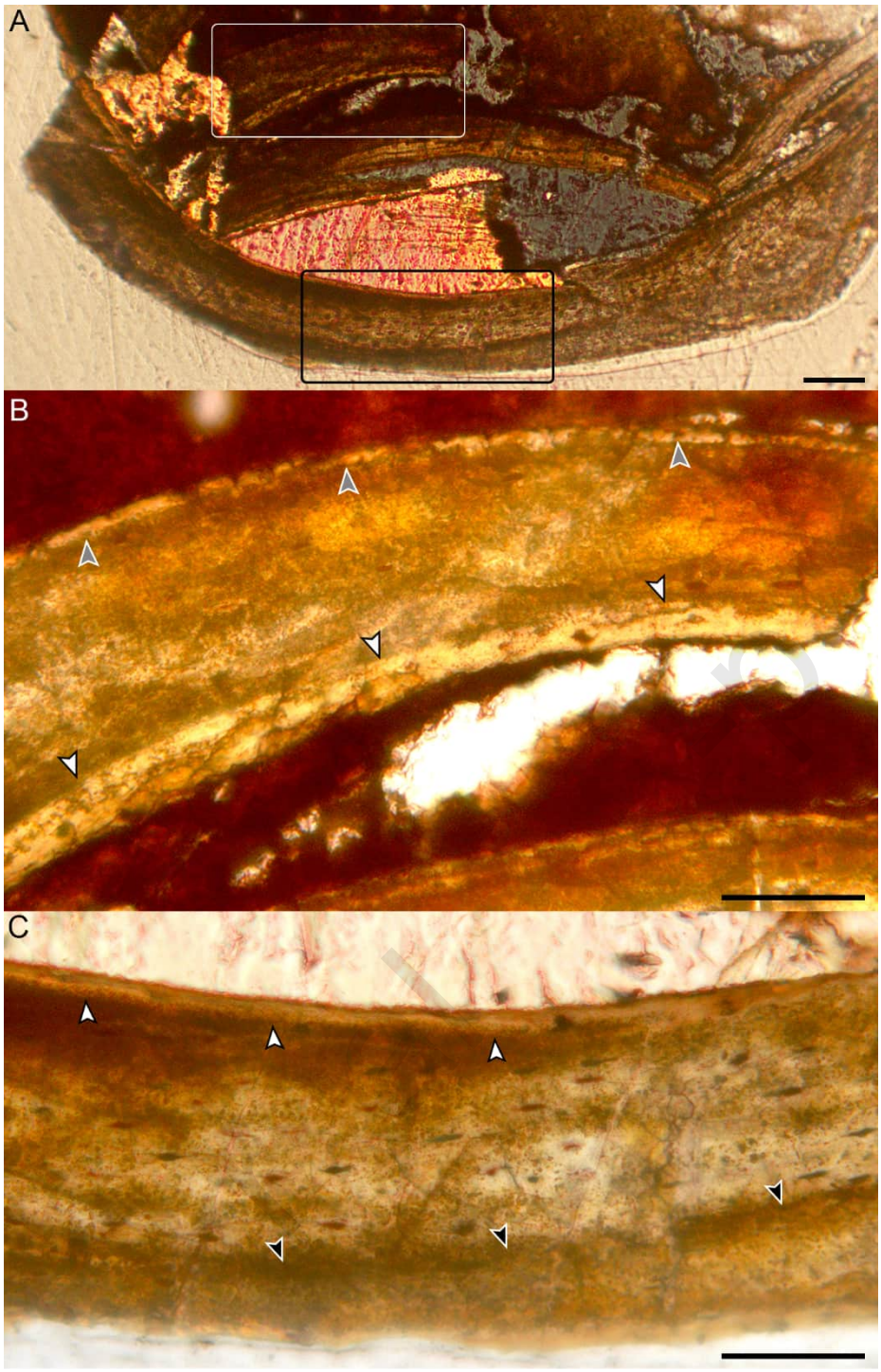
A
B
C

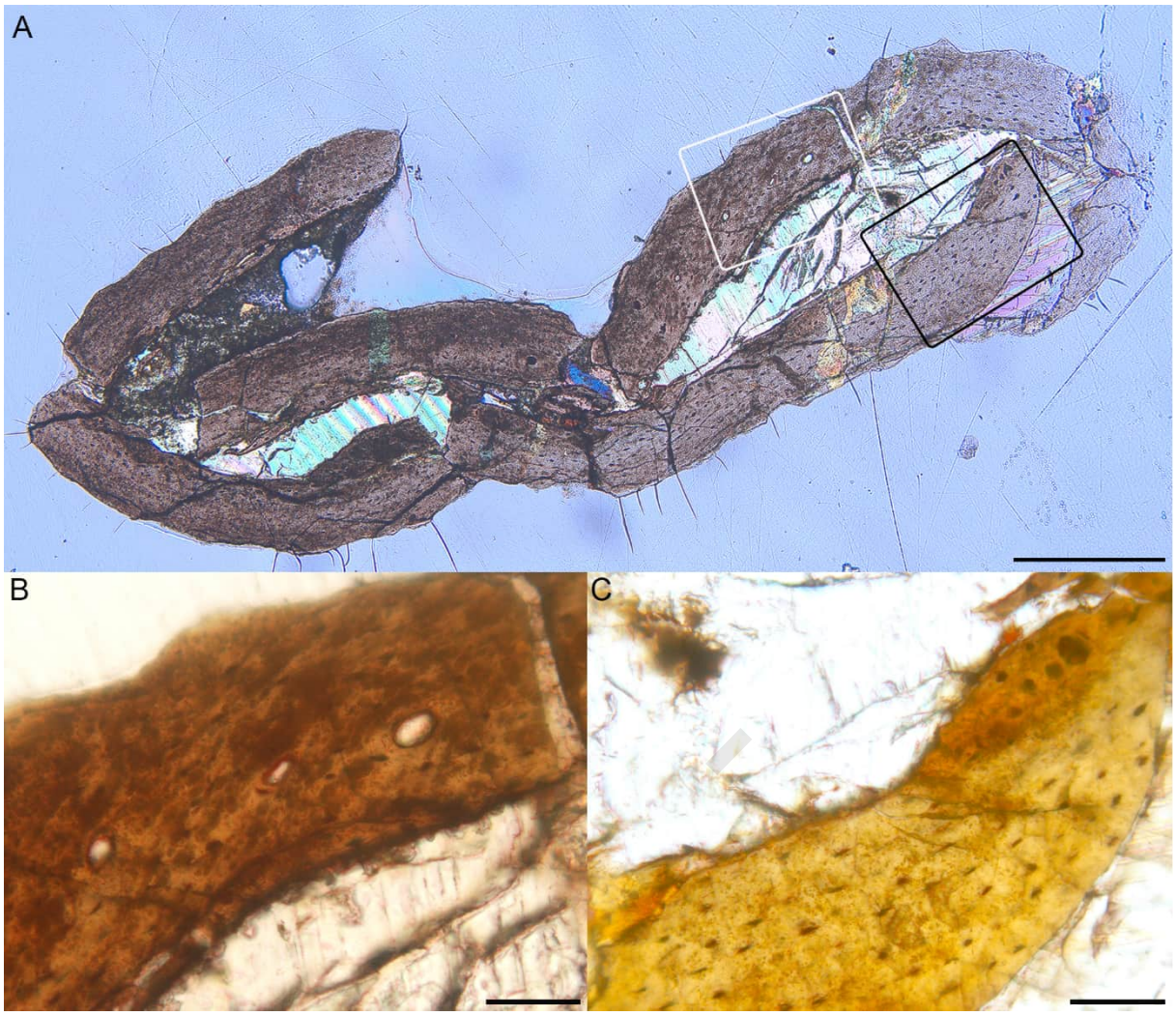
A
B
C

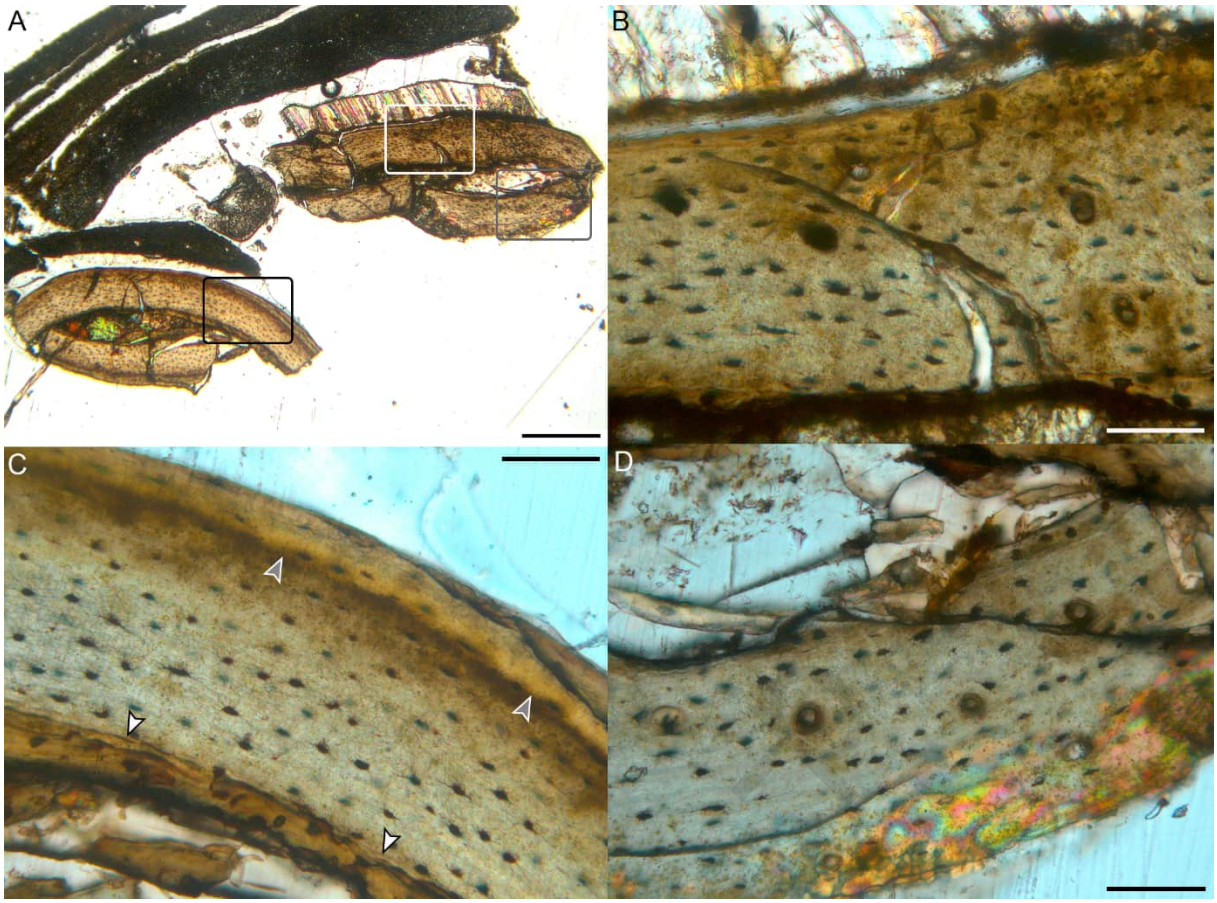
A
B
C
D

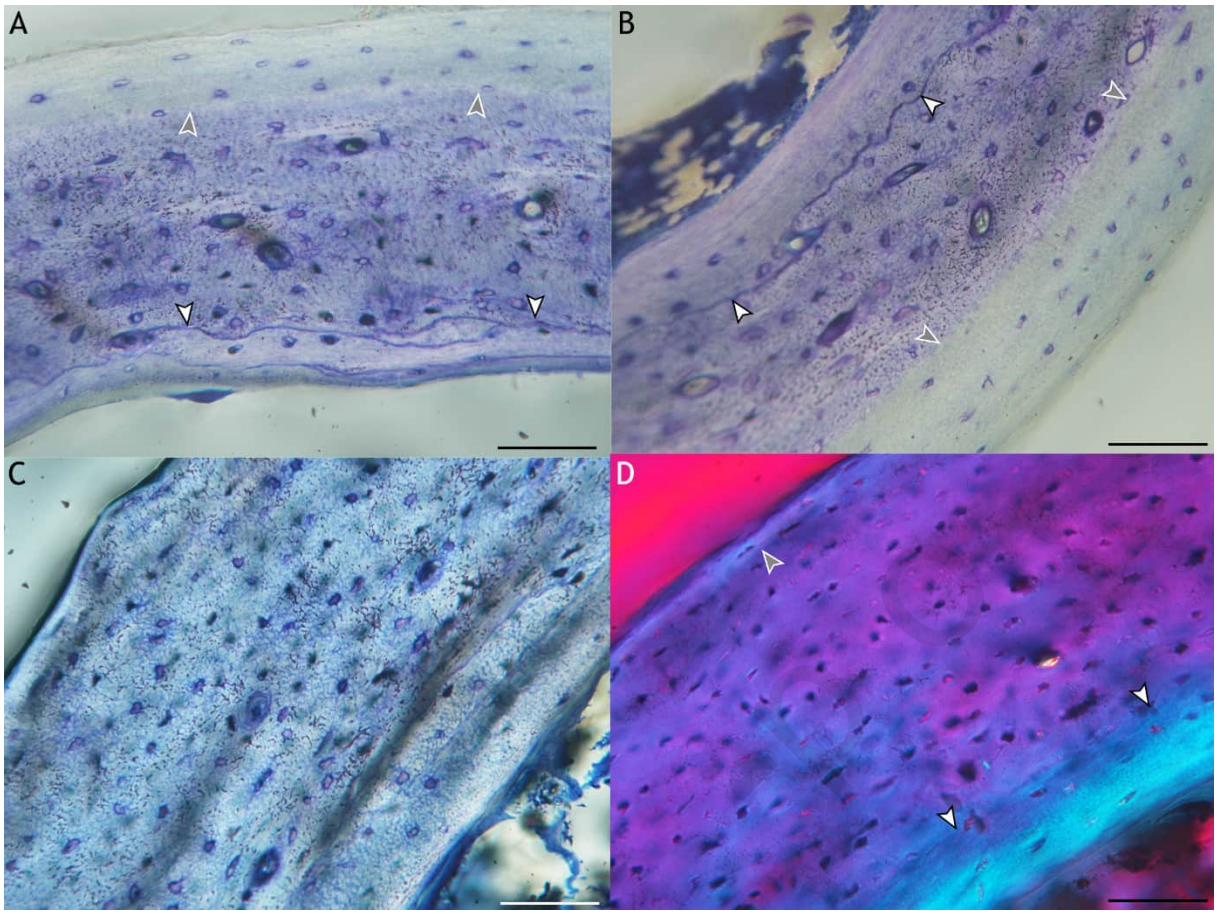
A
B
C
D